To appear in the Proceedings of ECCV'00, June, 2000

Monocular perception of biological motion – clutter and partial occlusion

Yang Song[1], Luis Goncalves[1], and Pietro Perona[1,2]

[1] California Institute of Technology, 136-93,
Pasadena, CA 91125, USA
[2] Università di Padova, Italy
{yangs, luis, perona}@vision.caltech.edu

Abstract. The problem of detecting and labeling a moving human body viewed monocularly in a cluttered scene is considered. The task is to decide whether or not one or more people are in the scene (detection), to count them, and to label their visible body parts (labeling).
It is assumed that a motion-tracking front end is supplied: a number of moving features, some belonging to the body and some to the background are tracked for two frames and their position and velocity is supplied (Johansson display). It is not guaranteed that all the body parts are visible, nor that the only motion present is the one of the body.
The algorithm is based on our previous work [12]; we learn a probabilistic model of the position and motion of body features, and calculate maximum-likelihood labels efficiently using dynamic programming on a triangulated approximation of the probabilistic model. We extend those results by allowing an arbitrary number of body parts to be undetected (e.g. because of occlusion) and by allowing an arbitrary number of noise features to be present. We train and test on walking and dancing sequences for a total of approximately 10^4 frames. The algorithm is demonstrated to be accurate and efficient.

1 Introduction

Humans have developed a remarkable ability in perceiving the posture and motion of the human body ('biological motion' in the human vision literature). Johansson [7] filmed people acting in total darkness with small light bulbs fixed to the main joints of their body. A single frame of a Johansson movie is nothing but a cloud of bright dots on a dark field; however, as soon as the movie is animated one can readily detect, count, segment a number of people in a scene, and even assess their activity, age and sex. Although such perception is completely effortless, our visual system is ostensibly solving a hard combinatorial problem (which dot should be assigned to which body part of which person?).

Perceiving the motion of the human body is difficult. First of all, the human body is richly articulated – even a simple stick model describing the pose of arms, legs, torso and head requires more than 20 degrees of freedom. The body moves in 3D which makes the estimation of these degrees of freedom a challenge in a monocular setting [4, 6]. Image processing is also a challenge: humans typically wear clothing which may be loose and textured. This makes it difficult to identify limb boundaries, and even more so to segment the main parts of the body. In a general setting all that can be extracted reliably from the images is patches of texture in motion. It is not so surprising after all that the human visual system has evolved to be so good at perceiving Johansson's stimuli.

Perception of biological motion may be divided into two phases: first detection and, possibly, segmentation; then tracking. Of the two, tracking has recently been object of much attention and considerable progress has been made [10, 9, 4, 5, 2, 14, 3]. Detection (given two frames: is there a human, where?), on the contrary, remains an open problem. In [12], we have focused on the Johannson problem proposing a method based on probabilistic modeling of human motion and on modeling the dependency of the motion of body parts with a triangulated graph, which makes it possible to solve the combinatorial problem of labeling in polynomial time. Excellent and efficient performance of the method has been demonstrated on a number of motion sequences. However, that work is limited to the case where there is no clutter (the only moving parts belong to the body, as in Johansson's displays). This is not a realistic situation: in typical scenes one would expect the environment to be rich of motion patterns (cars driving by, trees swinging in the wind, water rippling... as in Figure 1). Another limitation is that only limited amounts of occlusion is allowed. This is again not realistic: in the typical situations little more than half of the body is visible, the other half being self-occluded.

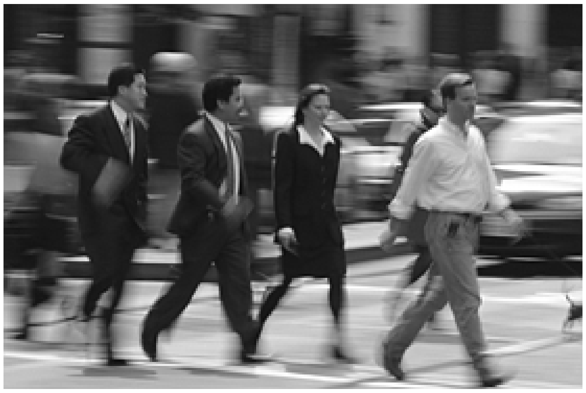

Fig. 1. Perception of biological motion in real scenes: one has to contend with a large amount of clutter (more than one person in the scene, other objects in the scene are also moving), and a large amount of self-occlusion (typically only half of the body is seen). Observe that segmentation (arm vs. body, left and right leg) is at best problematic.

We propose here a modification of our previous scheme [12] which addresses both the problem of clutter and of large occlusion. We conduct experiments to explore its performance vis a vis different types and levels of noise, variable amounts of occlusion, and variable numbers of human bodies in the scene. Both the detection performance and the labeling performance are assessed, as well as the performance in counting the number of people in the scene.

In section 2 we first introduce the problem and some notation, then propose our approach. In section 3 we explain how to perform detection. In section 4 a simple method for aggregating information over a number of frames is discussed. In section 5 we explain how to count how many people there may be in the picture. Section 6 contains the experiments.

2 Labeling

In the Johansson scenario, each body part appears as a single dot in the image plane. Our problem can then be formulated as follows: given the positions and velocities of a number of point-features in the image plane (Figure 2(a)), we want to find the configuration that is most likely to correspond to a human body. Detection is done based on how human-like the best configuration is.

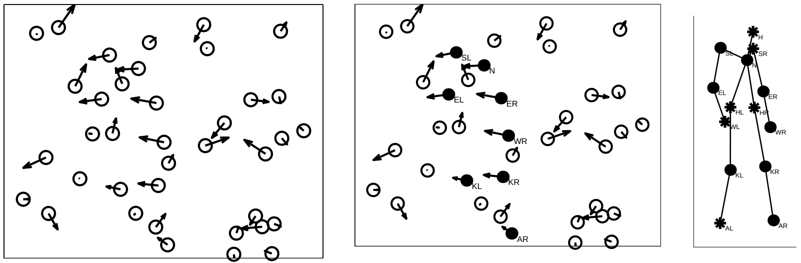

(a) (b) (c)

Fig. 2. Illustration of the problem. Given the position and velocity of point-features in the image plane (a), we want to find the best possible human configuration: filled dots in (b) are body parts and circles are background points. Arrows in (a) and (b) show the velocities. (c) is the full configuration of the body. Filled (blackened) dots represent the 'observed' points which appear in (b), and the '*'s are unobserved body parts. 'L' and 'R' in label names indicate left and right. H:head, N:neck, S:shoulder, E:elbow, W:wrist, H:hip, K:knee and A:ankle.

2.1 Notation

Suppose that we observe N points (as in Figure 2(a), where $N = 38$). We assign an arbitrary index to each point. Let $\mathcal{S}_{body} = \{LW, LE, LS, H \dots RA\}$ be the set of M body parts, for example, LW is the left wrist, RA is the right ankle, etc. Then:

$$i \in 1, \dots, N \qquad \text{Point index} \tag{1}$$

$$\overline{X} = [X_1, \dots, X_N] \qquad \text{Vector of measurements (position and velocity)} \tag{2}$$

$$\overline{L} = [L_1, \dots, L_N] \qquad \text{Vector of labels} \tag{3}$$

$$L_i \in \mathcal{S}_{body} \cup \{BG\} \qquad \text{Set of possible values for each label} \tag{4}$$

Notice that since there exist clutter points that do not belong to the body, the background label BG is added to the label set. Due to clutter and occlusion N is not necessarily equal to M (which is the size of $\mathcal{S}_{body}$). We want to find $\overline{L}^*$, over all possible label vectors $\overline{L}$, such that the posterior probability of the labeling given the observed data is maximized, that is,

$$\overline{L}^* = \arg\max_{\overline{L}\in\mathcal{L}} P(\overline{L}|\overline{X}) \tag{5}$$

where $P(\overline{L}|\overline{X})$ is the conditional probability of a labeling $\overline{L}$ given the data $\overline{X}$. Using Bayes' law:

$$P(\overline{L}|\overline{X}) = P(\overline{X}|\overline{L})\frac{P(\overline{L})}{P(\overline{X})} \tag{6}$$

If we assume that the priors $P(\overline{L})$ are equal for different labelings, then,

$$\overline{L}^* = \arg\max_{\overline{L}\in\mathcal{L}} P(\overline{X}|\overline{L}) \tag{7}$$

Given a labeling $\overline{L}$, each point feature i has a corresponding label L_i. Therefore each measurement X_i corresponding to body labels may also be written as X_{L_i}, i.e. the measurements corresponding to a specific body part associated with label L_i. For example if $L_i = LW$, i.e. the label corresponding to the left wrist is assigned to the ith point, then $X_i = X_{LW}$ is the position and velocity of the left wrist.

Let $\overline{\mathcal{L}}_{body}$ denote the set of body parts appearing in $\overline{L}$, $\overline{X}_{body}$ be the vector of measurements labeled as body parts, and $\overline{X}_{bg}$ be the vector of measurements labeled as background (BG). More formally,

$$\begin{aligned} \overline{\mathcal{L}}_{body} &= \{L_i; i = 1, \ldots, N\} \cap \mathcal{S}_{body} \\ \overline{X}_{body} &= [X_{i_1}, \ldots, X_{i_K}] \qquad \text{such that } \{L_{i_1}, \ldots, L_{i_K}\} = \overline{\mathcal{L}}_{body} \\ \overline{X}_{bg} &= [X_{j_1}, \ldots, X_{j_{N-K}}] \qquad \text{such that } L_{j_1} = \cdots = L_{j_{N-K}} = BG \end{aligned} \tag{8}$$

where K is the number of body parts present in $\overline{L}$.

If we assume that the position and velocity of the visible body parts is independent of the position and velocity of the clutter points, then,

$$P(\overline{X}|\overline{L}) = P_{\overline{\mathcal{L}}_{body}}(\overline{X}_{body}) \cdot P_{bg}(\overline{X}_{bg}) \tag{9}$$

where $P_{\overline{\mathcal{L}}_{body}}(\overline{X}_{body})$ is the marginalized probability density function of $P_{\mathcal{S}_{body}}$ according to $\overline{\mathcal{L}}_{body}$. If independent uniform background noise is assumed, then $P_{bg}(\overline{X}_{bg}) = (1/S)^{N-K}$, where $N-K$ is the number of background points, and S is the volume of the space X_i lies in, which can be obtained from the training set. In the following sections, we will address the issues of estimating $P_{\overline{\mathcal{L}}_{body}}(\overline{X}_{body})$ and finding the $\overline{L}^*$ with the highest likelihood.

2.2 Approximation of the foreground probability density function

If no body part is missing, we can use the method proposed in [12] to get the approximation of the foreground probability density $P_{\overline{\mathcal{L}}_{body}}(\overline{X}_{body})$. By using the kinematic chain structure of human body, the whole body can be decomposed as in Figure 3(a). If the appropriate conditional independence (Markov property) is valid, then

$$\begin{aligned}
&P_{\overline{\mathcal{L}}_{body}}(\overline{X}_{body}) \\
&= P_{\mathcal{S}_{body}}(X_{LW}, X_{LE}, X_{LS}, X_H \ldots X_{RA}) \\
&= P_{LW|LE,LS}(X_{LW}|X_{LE}, X_{LS}) \cdot P_{LE|LS,LH}(X_{LE}|\ldots) \cdot \ldots \\
&\cdot P_{RK,LA,RA}(X_{RK}, X_{LA}, X_{RA}) \\
&= \prod_{t=1}^{T-1} P_t(X_{A_t}|X_{B_t}, X_{C_t}) \cdot P_T(X_{A_T}, X_{B_T}, X_{C_T}) \qquad (10)
\end{aligned}$$

Where T is the number of triangles in the decomposed graph in Figure 3(a), t is the triangle index, and A_t is the first label associated to triangle t, etc.

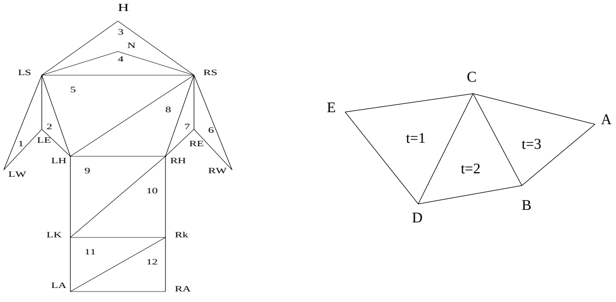

(a) (b)

Fig. 3. (a) One decomposition of the human body into triangles [12]. The label names are the same as in Figure 2. The numbers inside triangles give the order in which dynamic programming proceeds. (b) An illustrative example used in section 2.2.

If some body parts are missing, then the foreground probability density function is the marginalized version of the above equation – marginalization over the missing body parts. Marginalization should be performed so that it is a good approximation of the true marginal probability density function and allows efficient computation such as dynamic programming. We propose that doing the marginalization term by term (triangle by triangle) of equation (10) and then multiplying them together is a reasonable way to get such an approximation. The idea can be illustrated by a simple example as in Figure 3(b). Considering the joint probability density function of 5 random variables $P(A, B, C, D, E)$, if these random variables are conditionally independent as described in the graph of Figure 3 (b), then

$$P(A, B, C, D, E) = P(A, B, C)P(D|B, C)P(E|C, D) \qquad (11)$$

If A is missing, then the marginalized PDF is $P(B,C,D,E)$. If the conditional independence as in equation (11) can hold, then,

$$P(B,C,D,E) = P(B,C) \cdot P(D|B,C) \cdot P(E|C,D) \tag{12}$$

In the case of D missing, the marginalized PDF is $P(A,B,C,E)$. If we assume that E is conditionally independent of A and B given C, which is a more demanding conditional independence requirement with the absence of D compared to that of equation (11), then,

$$P(A,B,C,E) = P(A,B,C) \cdot 1 \cdot P(E|C) \tag{13}$$

Each term on the right hand sides of equations (12) and (13) is the marginalized version of its corresponding term in equation (11). Similarly, if some stronger conditional independence can hold, we can obtain an approximation of $P_{\overline{\mathcal{L}}_{body}}(\overline{X}_{body})$ by performing the marginalization term by term of equation (10). For example, considering triangle (A_t, B_t, C_t), $1 \leq t \leq T-1$, if all of A_t, B_t and C_t are present, then the tth term of equation (10) is $P_{A_t|B_t,C_t}(X_{A_t}|X_{B_t}, X_{C_t})$; if A_t is missing, the marginalized version of it is 1; if A_t and C_t are observed, but B_t is missing, it becomes $P_{A_t|C_t}(X_{A_t}|X_{C_t)})$; if A_t exists but both B_t and C_t missing, it is $P_{A_t}(X_{A_t})$. For the Tth triangle, if some body part(s) are missing, then the corresponding marginalized version of P_T is used. The foreground probability $P_{\overline{\mathcal{L}}_{body}}(\overline{X}_{body})$ can be approximated by the product of the above (conditional) probability densities. Note that if too many body parts are missing, the conditional independence assumptions of the graphical model will no longer hold; it is reasonable to assume that the wrist is conditionally independent of the rest of the body given the shoulder and elbow, but if both shoulder and elbow are missing, this is no longer true. Nevertheless, we will use independence as an approximation. All the above (conditional) probability densities (e.g. $P_{LW|LE,LS}(X_{LW}|X_{LE}, X_{LS})$) can be estimated from the training data.

2.3 Cost functions and comparison of two labelings

The best labeling $(\overline{L}^*)$ can be found by comparing the likelihood of all the possible labelings. To compare two labelings $\overline{L}^1$ and $\overline{L}^2$, if we can assume that the priors $P(\overline{L}^1)$ and $P(\overline{L}^2)$ are equal, then by equation (9),

$$\begin{aligned}
\frac{P(\overline{L}^1|\overline{X})}{P(\overline{L}^2|\overline{X})} = \frac{P(\overline{X}|\overline{L}^1)}{P(\overline{X}|\overline{L}^2)} &= \frac{P_{\overline{\mathcal{L}}^1_{body}}(\overline{X}^1_{body}) \cdot P_{bg}(\overline{X}^1_{bg})}{P_{\overline{\mathcal{L}}^2_{body}}(\overline{X}^2_{body}) \cdot P_{bg}(\overline{X}^2_{bg})} \\
&= \frac{P_{\overline{\mathcal{L}}^1_{body}}(\overline{X}^1_{body}) \cdot (1/S)^{N-K_1}}{P_{\overline{\mathcal{L}}^2_{body}}(\overline{X}^2_{body}) \cdot (1/S)^{N-K_2}} \\
&= \frac{P_{\overline{\mathcal{L}}^1_{body}}(\overline{X}^1_{body}) \cdot (1/S)^{M-K_1}}{P_{\overline{\mathcal{L}}^2_{body}}(\overline{X}^2_{body}) \cdot (1/S)^{M-K_2}}
\end{aligned} \tag{14}$$

where $\overline{\mathcal{L}}^1_{body}$ and $\overline{\mathcal{L}}^2_{body}$ are the sets of observed body parts for $\overline{L}^1$ and $\overline{L}^2$ respectively, K_1 and K_2 are the sizes of $\overline{\mathcal{L}}^1_{body}$ and $\overline{\mathcal{L}}^2_{body}$, and M is the total number of body parts ($M = 14$ here). $P_{\overline{\mathcal{L}}^i_{body}}(\overline{X}^i_{body})$, $i = 1, 2$, can be approximated as in section 2.2. From equation (14), the best labeling $\overline{L}^*$ is the $\overline{L}$ which can maximize $P_{\overline{\mathcal{L}}_{body}}(\overline{X}_{body}) \cdot (1/S)^{M-K}$. This formulation makes both search by dynamic programming and detection in different frames (possibly with different numbers of candidate features N) easy, as will be explained below.

The dynamic programming algorithm [1, 12] requires that the local cost function associated with each triangle (as in Figure 3(a)) should be comparable for different labelings: whether there are missing part(s) or not. Therefore we cannot only use the terms of $P_{\overline{\mathcal{L}}_{body}}(\overline{X}_{body})$, because, for example, as we discussed in the previous subsection, the t^{th} term of $P_{\overline{\mathcal{L}}_{body}}(\overline{X}_{body})$ is $P_{A_t|B_tC_t}(X_{A_t}|X_{B_t}, X_{C_t})$ when all the three parts are present and it is 1 when A_t is missing. It is unfair to compare $P_{A_t|B_tC_t}(X_{A_t}|X_{B_t}, X_{C_t})$ with 1 directly. At this point, it is useful to notice that in $P_{\overline{\mathcal{L}}_{body}}(\overline{X}_{body}) \cdot (1/S)^{M-K}$, for each unobserved (missing) body part ($M - K$ in total), there is a $1/S$ term. $1/S$ (S is the volume of the space X_{A_t} lies in) can be a reasonable local cost for the triangle with vertex A_t (the vertex to be deleted) missing because then for the same stage, the dimension of the domain of the local cost function is the same. Also, $1/S$ can be thought of as a threshold of $P_{A_t|B_tC_t}(X_{A_t}|X_{B_t}, X_{C_t})$, namely, if $P_{A_t|B_tC_t}(X_{A_t}|X_{B_t}, X_{C_t})$ is smaller than $1/S$, then the hypothesis that A_t is missing will win. Therefore, the local cost function for the t^{th} ($1 \leq t \leq T - 1$) triangle can be approximated as follows:
- if all the three body parts are observed, it is $P_{A_t|B_tC_t}(X_{A_t}|X_{B_t}, X_{C_t})$;
- if A_t is missing or two or three of A_t, B_t, C_t are missing, it is $1/S$;
- if either B_t or C_t is missing and the other two body parts are observed, then it is $P_{A_t|C_t}(X_{A_t}|X_{C_t})$ or $P_{A_t|B_t}(X_{A_t}|X_{B_t})$.

The same idea can be applied to the last triangle T. These approximations are to be validated in experiments. Notice that when two body parts in a triangle are missing, only velocity information for the third body part is available since we use relative positions. The velocity of a point alone doesn't have much information, so for two parts missing, we use the same cost function as the case of three body parts missing.

With the local cost functions defined above, dynamic programming can be used to find the labeling with the highest $P_{\overline{\mathcal{L}}_{body}}(\overline{X}_{body}) \cdot (1/S)^{M-K}$. The computational complexity is on the order of $M * N^3$.

3 Detection

Given a hypothetical labeling $\overline{L}$, the higher $P(\overline{X}|\overline{L})$ is, the more likely it is that the associated configuration of features represents a person. The labeling $\overline{L}^*$ with the highest $P_{\overline{\mathcal{L}}_{body}}(\overline{X}_{body}) \cdot (1/S)^{M-K}$ provides us with the most human-like configuration out of all the candidate labelings. Note that since the dimension of the domain of $P_{\overline{\mathcal{L}}_{body}}(\overline{X}_{body}) \cdot (1/S)^{M-K}$ is fixed regardless of the number of candidate features and the number of missing body parts in the labeling $\overline{L}$, we can directly compare the likelihoods of different hypotheses, even hypotheses from different images.

In order to perform detection we first get the most likely labeling, then compare the likelihood of this labeling to a threshold. If the likelihood is higher than the threshold, then we will declare that a person is present. This threshold needs to be set based on experiments, to ensure the best trade-off between false acceptance and false rejection errors.

4 Integrating temporal information [11]

So far, we have only assumed that we may use information from two consecutive frames, from which we obtain position and velocity of a number of features. In this section we would like to extend our previous results to the case where multiple frames are available. However, in order to maintain generality we will assume that tracking across more than 2 frames is impossible. This is a simplified model of the situation where, due to extreme body motion or to loose and textured clothing, tracking is extremely unreliable and each individual feature's lifetime is short.

Let $P(O|\overline{X})$ denote the probability of the existence of a person given $\overline{X}$. From equation (14) and the previous section, we use the approximation: $P(O|\overline{X})$ is proportional to $\Gamma(\overline{X}|\overline{L}^*)$ defined as $\Gamma(\overline{X}|\overline{L}^*) \overset{\mathrm{def}}{=} \max_{\overline{L}\in\mathcal{L}} P_{\overline{\mathcal{L}}_{body}}(\overline{X}_{body}) \cdot (1/S)^{M-K}$, where $\overline{L}^*$ is the best labeling found from $\overline{X}$. Now if we have n observations $\overline{X}_1, \overline{X}_2, \ldots, \overline{X}_n$, then the decision depends on:

$$\begin{aligned} & P(O|\overline{X}_1, \overline{X}_2, \ldots, \overline{X}_n) \\ = {} & P(\overline{X}_1, \overline{X}_2, \ldots, \overline{X}_n|O) \cdot P(O)/P(\overline{X}_1, \overline{X}_2, \ldots, \overline{X}_n) \\ = {} & P(\overline{X}_1|O)P(\overline{X}_2|O)\ldots P(\overline{X}_n|O) \cdot P(O)/P(\overline{X}_1, \overline{X}_2, \ldots, \overline{X}_n) \end{aligned} \qquad (15)$$

The last line of equation (15) holds if we assume that $\overline{X}_1, \overline{X}_2, \ldots, \overline{X}_n$ are independent. Assuming that the priors are equal, $P(O|\overline{X}_1, \overline{X}_2, \ldots, \overline{X}_n)$ can be represented by $P(\overline{X}_1|O)\ldots P(\overline{X}_n|O)$, which is proportional to $\prod_{i=1}^{n} \Gamma(\overline{X}_i|\overline{L}_i^*)$. If we set up a threshold for $\prod_{i=1}^{n} \Gamma(\overline{X}_i|\overline{L}_i^*)$, then we can do detection given $\overline{X}_1, \overline{X}_2, \ldots, \overline{X}_n$.

5 Counting

Counting how many people are in the scene is also an important task since images often have multiple people in them. By the method described above, we can first get the best configuration to see if it could be a person. If so, all the points belonging to the person are removed and the next best labeling can then be found from the rest of points. We repeat until the likelihood of the best configuration is smaller than a threshold. Then the number of configurations with likelihood greater than the threshold is the number of people in the scene.

6 Experiments

In this section we explore experimentally the performance of our system. The data were obtained from a 60 Hz motion capture system. The motion capture system can provide us with labeling for each frame which can be used as ground truth. In our experiments, we assumed that both position and velocity were available for each candidate point. The velocity was obtained by subtracting the positions in two consecutive frames.

Two different types of motions were used in our experiments, walking and dancing. Figure 4 shows sample frames of these two motions.

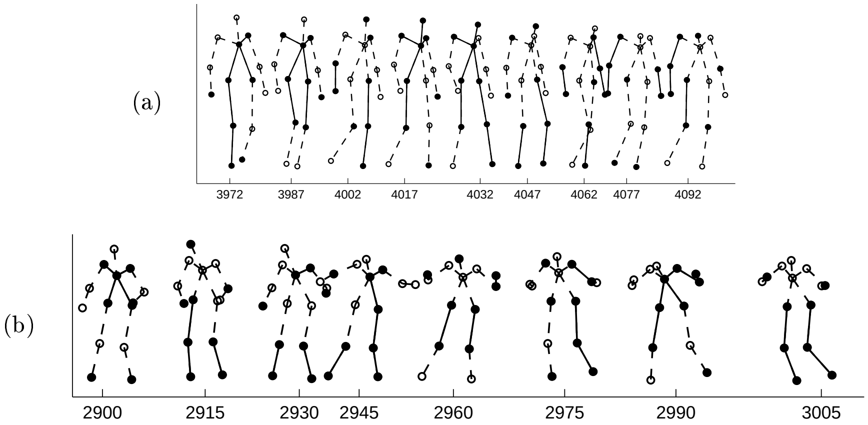

Fig. 4. Sample frames. (a) a walking sequence; (b) a dancing sequence. Eight Filled dots denote the eight observed body parts; the open circles mark points that are actually missing (not available to the program). The numbers along the horizontal axes indicate the frame numbers.

6.1 Training of the probabilistic models

The probabilistic models were trained separately for walking and dancing, and in each experiment the appropriate model was used. For the walking action, two sequences of 7000 frames were available. The first sequence was used for training, and the second sequence for testing. For the dancing action, one sequence of 5000 frames was available; the first half was used for training, and the second half for testing.

The training was done by estimating the joint (or conditional) probabilistic density functions (pdf) for all the triplets as described in section 2. For each triplet, position information was expressed within a local coordinate frame, i.e. relative positions, and velocities were absolute ones. As in [12], we assumed that all the pdfs were Gaussian, and the parameters for the Gaussian distribution were estimated from the training set.

6.2 Detection

In this experiment, we test how well our method can distinguish whether or not a person is present in the scene (Figure 2). We present the algorithm with two types of inputs (presented randomly in equal proportions); in one case only clutter (background) points are present, in the other body parts from the walking sequence are superimposed on the clutter points. We call 'detection rate' the fraction of frames containing a body that is recognized correctly. We call 'false alarm rate' the fraction of frames containing only clutter where our system detects a body.

We want to test the detection performance when only part of the whole body (with 14 body parts in total) can be seen. We generated the signal points (body parts) in the following way: for a fixed number of signal points, we randomly selected which body parts would be used in each frame (actually pair of frames, since consecutive frames were used to estimate the velocity of each body part). So in principle, each body part has an equal chance to be represented, and as far as the decomposed body graph is concerned, all kinds of graph structures (with different body parts missing) can be tested.

The positions and velocities of clutter (background) points were independently generated from uniform probability densities. For positions, we used the leftmost and rightmost positions of the whole training sequence as the horizontal range, and highest and lowest body part positions as the vertical range. For velocities, the possible range was inside a circle in velocity space (horizontal and vertical velocities) with radius equal to the maximum magnitude of body part velocities in the training sequences. Figure 2 (a) shows a frame with 8 body parts and 30 added background points with arrows representing velocities.

The six solid curves of Figure 5 (a) are the receiver operating characteristics (ROCs) obtained from our algorithm when the 'positive' test images contained 3 to 8 signal points with 30 added background points and the 'negative' test images contained 30 background points. The more signal points, the better the ROC. With 30 background points, when the number of signal points is more than 8, the ROCs are almost perfect.

When using the detector in a practical situation, some detection threshold needs to be set; if the likelihood of the best labeling exceeds the threshold, a person is deemed to be present. Since the number of body parts is unknown beforehand, we need to fix a threshold that is independent of (and robust with respect to) the number of body parts present in the scene. The dashed line in Figure 5 (a) shows the overall ROC of all the frames used for the six ROC curves in solid lines. We took the threshold when $P_{detect} = 1 - P_{false-alarm}$ on it as our threshold. The star ('*') point on each solid curve shows the point corresponding to that threshold. Figure 5 (b) shows the relation between detection rate and number of body parts displayed with regard to the fixed threshold. The false alarm rate is 12.97%.

When the algorithm can correctly detect whether there is a person, it doesn't necessarily mean that all the body parts are correctly labeled. Therefore we also studied the correct label rate when a person is correctly detected. Figure 5 (c) shows the result. While the detection rate is constant (with no errors) with 8 or more body parts visible, the correct label rate increases with the number of body parts. The correct label rates here are smaller than in [12] since we have less signal points but many more background points.

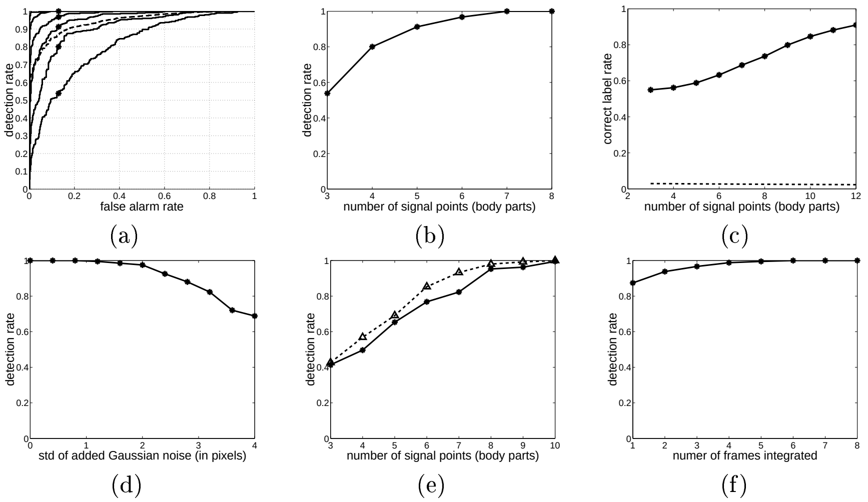

(a) (b) (c)

(d) (e) (f)

Fig. 5. (a) to (e) are detection results on 2 frames only, and (f) shows the result of using multiple frames. (a) ROC curves. Solid lines: 3 to 8 out of 14 body parts with 30 background points vs. 30 background points only. The more signal points, the better the ROC. Dashed line: overall ROC considering all the frames. The threshold corresponding to $P_D = 1 - P_{FA}$ on it was used for later experiments. The stars ('*') on the solid curves are the points corresponding to that threshold. (b) detection rate vs. number of body parts displayed with regard to the fixed threshold as in (a). The false alarm rate is 12.97%. (c) The solid line is correct label rate vs. number of body parts when a person is correctly detected. The chance level is shown in dashed line. (d) the detection rate vs. standard deviation (in pixels) when Gaussian noise was added to positions, using displays composed of 8 signal points and 30 background points in each frame. The standard deviation of the velocity error was one tenth of that of the position error. The detection threshold is the same as (b) and (c), with the false alarm rate 12.97%. (e) results for biological clutter (background points were obtained from the walking sequences): detection rate vs. number of signal points. Solid line (with stars): with 30 added background points, false alarm rate is 24.19%; Dashed line (with triangles): with 20 added background points, false alarm rate is 19.45%. (f) detection rate (when $P_{detect} = 1 - P_{false-alarm}$) vs. number of frames used with only 5 body parts present.

The data used above were acquired by an accurate motion capture system where markers were used to identify important features. In image sequences where people do not wear markers, candidate features can be obtained from a motion detector/feature tracker ([11, 13]), where extra measurement noise may be introduced. To test the performance of our method under that situation, independent Gaussian noise was added to the position and velocity of the signal points (body parts). We experimented with displays composed of 8 signal points and 30 background points in each frame. Figure 5 (d) shows the detection rate (with regard to the same threshold as Figure 5(b) and (c)) vs. standard deviation (in pixels) of added Gaussian noise to positions. The standard deviation of noise added to velocities is one tenth of that of positions, which reflects the fact that the position error, due to the inaccurate localization of a feature by a tracking algorithm ([11, 13]), is usually much larger than the velocity error which is due to the tracking error from one frame to the next.

We also tested our method by using biological clutter, that is, the background points were generated by independently drawing points (with position and velocity) of randomly chosen frames and body parts from the walking sequence. Figure 5(e) shows the results.

6.3 Using temporal information

The detection rate improves by integrating information over time as discussed in section 4. We tested this using displays composed of 5 signal points and 30 background points (the 5 body parts present in each frame were chosen randomly and independently). The results are shown in Figure 5(f).

6.4 Counting

We call 'counting' the task of finding how many people are present in a scene. Our stimuli with multiple persons were obtained in the following way. A person was generated by randomly choosing a frame from the sequence, and several frames (persons) can be superimposed together in one image with the position of each person selected randomly but not overlapped with each other. The statistics of background features was similar to that in section 6.2 (Figure 5(a)), but with the positions distributed on a window three times as wide as that in Figure 2 (a). Figure 6(a) gives an example of images used in this experiment, with three persons (six body parts each) and sixty background points.

Our stimuli contained from zero to three persons. The threshold from Figure 5(a) was used for detection. If the probability of the configuration found was above the threshold, then it was counted as a person. The curves in Figure 6(b) show the correct count rate vs. the number of signal points. To compare the results conveniently, we used the same number of body parts for different persons in one image (but the body parts present were randomly chosen). The solid line represents counting performance when one person was present in each image, the dashed line with circles is for stimuli containing two persons, and the dash-dot line with triangles is for three persons. If there was no person in the image, the correct rate was 95%. From Figure 6(b), we see that the result for displays containing fewer people is better than that with more people, especially when the number of observed body parts is small. We can explain it as follows. If the probability of counting one person correctly is P, then the probability of counting n people correctly is P^n if the detection of different people is independent. For

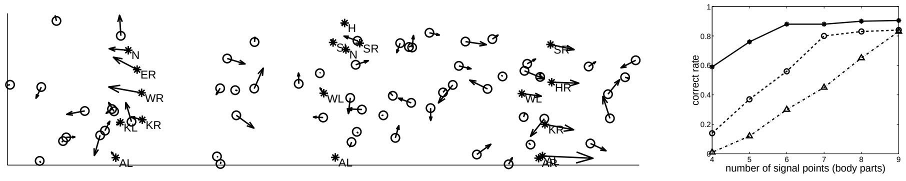

(a) (b)

Fig. 6. (a) One sample image of counting experiments. '*'s denote body parts and 'o's are background points. There are three persons (six body parts for each person) with sixty superimposed background points. Arrows are the velocities. (b) Results of counting experiments: correct rate vs. number of body parts. Solid line (with solid dots): one person; dashed line (with open circles): two persons; dash-dot line (with triangles): three persons. Detection of a person is with regard to the threshold chosen from Figure 5(a). For that threshold the correct rate for recognizing that there is no person in the scene is 95%.

example, in the case of four body parts, for one person the correct rate is 0.6, then the correct rate for counting three person is $0.6^3 = 0.216$. This is just an approximation since body parts from different persons may be very close and the body part of one person may be perceived as belonging to another. Furthermore, the assumption of independence is also violated since once a person is detected the corresponding body parts are removed from the scene in order to detect subsequent people.

6.5 Experiments on dancing sequence

In the previous experiments, walking sequences were used as our data. In this section, we tested our model on a dancing sequence. Results are shown in Figure 7. The signal points (body parts) were from the dancing sequence and the clutter points were generated the same way as in section 6.2 (Figure 5(a)).

7 Conclusions

We have presented a method for detecting, labeling and counting biological motion in a Johansson-like sequence. We generalize our previous work [12] by extending the technique to work on arbitrary amounts of clutter and occlusion.

We have tested our implementation on two kinds of moving sequences (walking and dancing) and demonstrated that it performs well under conditions of clutter and occlusion that are possibly more challenging than one would expect in a typical real-life scenario. The motion clutter we injected in our displays was designed to resemble the motion of individual body parts, the number of noise points in our experiments far exceeded the number of signal points, the number of undetected/occluded signal features in some experiments exceeded the number of detected features. Just to quote one significant performance figure: 2-frame detection rate is better than 90% when 6 out of 14 body parts are seen

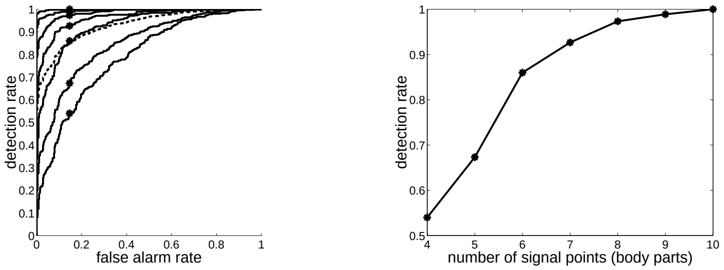

(a) (b)

Fig. 7. Results of dancing sequences. (a) Solid lines: ROC curves for 4 to 10 body parts with 30 background points vs. 30 background points only. The more signal points, the better the ROC. Dashed line: overall ROC considering all the frames used in seven solid ROCs. The threshold corresponding to $P_D = 1 - P_{FA}$ on this curve was used for (b). The stars ('*') on the solid curves are the points corresponding to that threshold. (b) detection rate vs. the number of body parts displayed with regard to the fixed threshold. The false alarm rate is 14.67%. Comparing with the results in Figure 5 (a, b), we can see that more body parts must be observed during the dancing sequence to achieve the same detection rate as with the walking sequences, which is expected since the motion of dancing sequences is more active and harder to model. Nevertheless, the ROC curve with 10 out of 14 body parts present is nearly perfect.

within 30 clutter points (see Figure 5(b)). When the number of frames considered exceeds 5 then performance quickly reaches 100% correct (see Figure 5(f)). This means that even in high-noise conditions detection is flawless in 100ms or so (considering a 60 Hz imaging system), a figure comparable to the alleged performance of the human visual system [8]. Moreover, our algorithm is computationally efficient, taking order of 1 second in our Matlab implementation on a regular Pentium computer, which gives significant hope for a real-time C implementation on the same computer.

The next step in our work is clearly the application of our system to real image sequences, rather than Johansson displays. We anticipate using a simple feature/patch detector and tracker in order to provide the position-velocity measurements that are input in our system. Since our system can work with features that have a short life-span (in the limit 2-frame) this should be feasible without modifying the overall approach. A first set of experiments is described in [11]. Comparing in detail the performance of our algorithm with the human visual system is another avenue that we intend to pursue.

Acknowledgments

Funded by the NSF Engineering Research Center for Neuromorphic Systems Engineering (CNSE) at Caltech (NSF9402726), and by an NSF National Young Investigator Award to PP (NSF9457618).

References

1. Y. Amit and A. Kong, “Graphical templates for model registration”, *IEEE Transactions on Pattern Analysis and Machine Intelligence*, 18:225–236, 1996.
2. C. Bregler and J. Malik, “Tracking people with twists and exponential maps”, In *Proc. IEEE CVPR*, pages 8–15, 1998.
3. D. Gavrila, “The visual analysis of human movement: A survey”, *Computer Vision and Image Understanding*, 73:82–98, 1999.
4. L. Goncalves, E. Di Bernardo, E. Ursella, and P. Perona, “Monocular tracking of the human arm in 3d”, In *Proc. 5th Int. Conf. Computer Vision*, pages 764–770, Cambridge, Mass, June 1995.
5. I. Haritaoglu, D.Harwood, and L.Davis, “Who, when, where, what: A real time system for detecting and tracking people”, In *Proceedings of the Third Face and Gesture Recognition Conference*, pages 222–227, 1998.
6. N. Howe, M. Leventon, and W. Freeman, “Bayesian reconstruction of 3d human motion from single-camera video”, *Tech. Rep. TR-99-37, a Mitsubishi Electric Research Lab*, 1999.
7. G. Johansson, “Visual perception of biological motion and a model for its analysis”, *Perception and Psychophysics*, 14:201–211, 1973.
8. P. Neri, M.C.Morrone, and D.C.Burr, “Seeing biological motion”, *Nature*, 395:894–896, 1998.
9. J.M. Rehg and T. Kanade, “Digiteyes: Vision-based hand tracking for human-computer interaction”, In *Proceedings of the workshop on Motion of Non-Rigid and Articulated Bodies*, pages 16–24, November 1994.
10. K. Rohr, “Incremental recognition of pedestrians from image sequences”, In *Proc. IEEE Conf. Computer Vision and Pattern Recognition*, pages 8–13, New York City, June, 1993.
11. Y. Song, X. Feng, and P. Perona, “Towards detection of human motion”, *To appear in IEEE Conference on Computer Vision and Pattern Recognition*, 2000.
12. Y. Song, L. Goncalves, E. Di Bernardo, and P. Perona, “Monocular perception of biological motion - detection and labeling”, In *Proceedings of International Conference on Computer Vision*, pages 805–812, Sept 1999.
13. C. Tomasi and T. Kanade, “Detection and tracking of point features”, *Tech. Rep. CMU-CS-91-132,Carnegie Mellon University*, 1991.
14. S. Wachter and H.-H. Nagel, “Tracking persons in monocular image sequences”, *Computer Vision and Image Understanding*, 74:174–192, 1999.